Snake states and their symmetries in graphene

Yang Liu,[1] Rakesh P. Tiwari,[2] Matej Brada,[1] C. Bruder,[2] F. V. Kusmartsev,[1] and E. J. Mele[1,3,*]

[1]*Department of Physics, Loughborough University LE11 3TU, United Kingdom*
[2]*Department of Physics, University of Basel, Klingelbergstrasse 82, CH-4056 Basel, Switzerland*
[3]*Department of Physics and Astronomy, University of Pennsylvania, Philadelphia, Pennsylvania 19104, USA*

Snake states are open trajectories for charged particles propagating in two dimensions under the influence of a spatially varying perpendicular magnetic field. In the quantum limit they are protected edge modes that separate topologically inequivalent ground states and can also occur when the particle density rather than the field is made nonuniform. We examine the correspondence of snake trajectories in single-layer graphene in the quantum limit for two families of domain walls: (a) a uniform doped carrier density in an antisymmetric field profile and (b) antisymmetric carrier distribution in a uniform field. These families support different internal symmetries but the same pattern of boundary and interface currents. We demonstrate that these physically different situations are gauge equivalent when rewritten in a Nambu doubled formulation of the two limiting problems. Using gauge transformations in particle-hole space to connect these problems, we map the protected interfacial modes to the Bogoliubov quasiparticles of an interfacial one-dimensional p-wave paired state. A variational model is introduced to interpret the interfacial solutions of both domain wall problems.

I. INTRODUCTION

A charged particle moving in two dimensions under the influence of a spatially varying perpendicular magnetic field can exhibit snake state trajectories. These are open two-dimensional orbits perpendicular to the direction of the magnetic field gradient. Snake trajectories occur in both the classical and quantum limits of this problem and are of fundamental interest with potential applications for electron transport in multidomain ferromagnets, two-dimensional electron gases [1,2], and in nanomaterials like graphene [3–5]. In the quantum limit the snake states can be interpreted as the protected modes that occur at domain walls that separate topologically mismatched gapped ground states. This picture suggests that snake trajectories can arise even in a *uniform* magnetic field if the particle density is suitably modulated laterally, e.g., by electrostatic gating patterned to form interfaces between distinct quantum Hall ground states.

Indeed exactly this possibility has been explored theoretically [6–9] and examined experimentally for graphene in a uniform perpendicular magnetic field via measurements of the Hall conductance and of Fabry-Perot-like oscillations in the interedge conductance across graphene *pn* junctions [10,11]. Graphene is an excellent candidate for this application because it can be electrostatically switched from *n* to *p* carrier types and studied in the ballistic transport regime [12]. Semiclassical analysis of graphene *pn* junctions in a uniform magnetic field has been a subject of many studies [13–15]. The converse problem of snake trajectories for a uniform carrier density in a spatially varying magnetic field is even more technically challenging and it has not been examined experimentally (for a theoretical discussion see Ref. [16]). On the other hand, a variant of this latter problem *is* routinely encountered in present-day experimental environments. In single-layer graphene subject to elastic lattice strains, the low-energy

electronic structure is described by a Dirac Hamiltonian containing a strain-induced gauge field that mimics the effects of a perpendicular (albeit valley antisymmetric) magnetic field. For generic smoothly varying strain fields the presence of nodal lines that separate regions of "positive" and "negative" pseudomagnetic field in a single valley is a nearly unavoidable consequence of the symmetry of this strain coupling.

The "antisymmetric B" and "antisymmetric doping (V)" problems break both time-reversal symmetry $\mathcal{T}$ (due to the presence of a magnetic field) and particle-hole symmetry Ξ (they require a nonzero carrier density). Nonetheless they retain different composite symmetry operations that combine these discrete symmetries with twofold rotation about the layer normal $\mathcal{R}_z$: the former problem is symmetric under $\mathcal{R}_z\mathcal{T}$ and the latter under $\mathcal{R}_z\Xi$. This difference manifests itself in many of the spectral properties presented in Sec. II. In fact, this distinction persists even into the classical limit, and reflects the different underlying dynamics of these two problems. In the antisymmetric-B problem a snake state trajectory arises from the compensation of the circulation of cyclotron orbits in regions where the magnetic field is reversed. In the antisymmetric V it arises from one-sided skipping orbits due to an electric field at the interface of a *pn* junction. It is perhaps surprising that these problems exhibit the *same* pattern of boundary and interface currents. This can be understood as a consequence of confinement of these boundary modes at the interface between topologically mismatched gapped ground states on either side of the interface. It is therefore of interest to understand precisely how these different problems are related in the bulk. In this paper we observe that these two situations are in fact gauge equivalent representations of the same problem. However, our demonstration of this equivalence requires that we extend both problems in a Nambu-doubled formulation, explicitly restoring particle hole symmetry about a nonzero chemical potential. In this doubled representation we find that the problems are interconverted by local gauge transformations exploiting the particle and hole degrees of freedom in the Nambu basis. Among the insights provided

---

*mele@physics.upenn.edu

by this approach, we observe that the interfacial degrees of freedom common to the two problems (the snake states) are mapped to a model for the Bogoliubov quasiparticles in a one-dimensional superconductor along the tangent line that supports a "*p*-wave" pairing field.

This paper is organized as follows. In Sec. II we begin by comparing the spectra for antisymmetrically doped graphene (a *pn* junction) in uniform field with the spectrum for uniform doping in an antisymmetric field. In Sec. III we present a family of local gauge transformations that allow one to map one problem onto the other. In Sec. IV we implement this procedure for the case of the graphene *pn* junction and analyze the structure of the uniformly doped antisymmetric field problem to which it maps. In Sec. V we present a topological analysis of the ground state manifolds in these models, concluding that they are the same and are members of the Altland-Zirnbauer chiral symmetry class C, i.e., they are indexed by even integer-valued winding numbers. In Sec. VI we use a variational approach to determine the spatial structure of the interface modes.

II. SPECTRA OF THE FOLDED GRAPHENE AND *pn* JUNCTION IN MAGNETIC FIELD

We consider snake state solutions in two limits of a tight-binding theory for electrons on a honeycomb lattice. The Hamiltonian is

$$\mathcal{H} = \sum_i (V_i - \mu)(c_i^\dagger c_i - 1/2) + \sum_{\langle i,j \rangle} t e^{i\varphi_{ij}} c_i^\dagger c_j + \text{H.c.}, \quad (1)$$

where $\varphi_{i,j} = (e/\hbar) \int_i^j \vec{A} \cdot d\vec{\ell}$ is the Peierls phase accumulated in a (possibly nonconstant) perpendicular magnetic field B_i. We adopt a coordinate system where the scalar potential V_i and the vector potential $\vec{A}_i$ are spatially varying in the x direction and constant along y. The chemical potential μ is set so that the left and right sectors are simultaneously gapped. The calculations are carried out for "zigzag" interfaces, where a domain wall at $x = 0$ is tangent to a primitive translation vector along y. We examine two limiting domain wall geometries. In the first we assume that the system is uniformly doped, say p type on both sides of an interface where $B(x)$ changes sign. In the second we consider the complementary case where the B field is uniform (or at least a symmetric function of x with no sign changes), and instead the external scalar potential $V(x)$ with zero mean changes its sign on an interface defining a *pn* junction. We show that the edge-state solutions for these two limits are the same despite the different microscopic dynamics. This manifests a topological equivalence of their bulk ground states. Indeed we find that these can be mapped into each other by gauge transformations that mix the particle and hole degrees of freedom when the problem is rewritten in a Nambu particle-hole basis. This leads to the possibility of inventing architectures that simulate unusual ballistic transport effects like Andreev reflection even in the absence of a physical superconducting condensate. In the following we will first discuss the two limits separately and then analyze their gauge equivalence.
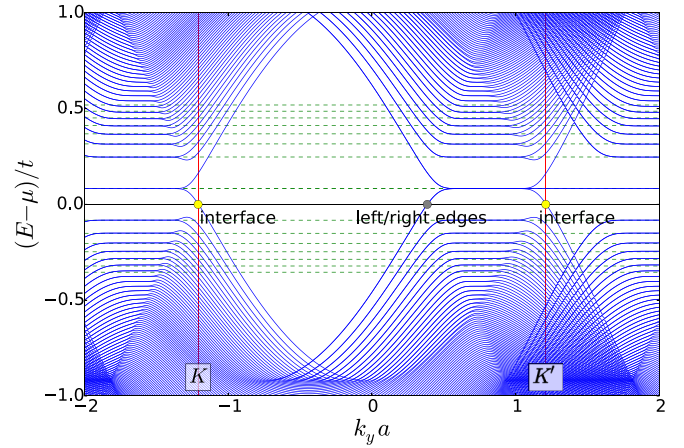

FIG. 1. (Color online) Numerically calculated spectrum for graphene with uniform doping in an antisymmetric magnetic field profile. We plot E-μ as a function of $k_y a$, where a is the interatomic distance in graphene, and assume p-type doping (i.e., $\mu = 0$, and a uniform scalar potential V that shifts the system away from neutrality). The spectrum shows four dispersing features at the Fermi energy: two with "positive" velocity on the outer edges, and a pair of modes with "negative" velocity in the domain wall. The flat band that extends from the K to K' points is the surface state for a zigzag edge. The horizontal dashed lines show the dispersionless bulk Landau levels for a Dirac system.

A. Antisymmetric *B*, symmetric *V*

We assume that the system is uniformly slightly doped p type and has an antisymmetric magnetic field profile $B(x) = B_o \tanh(x/\ell)$. The spectrum for this problem is displayed in Fig. 1. The vertical red lines denote the projections of the bulk K and K' Dirac points, i.e., in the absence of a field these are the interface-projected locations of the bulk gap closures.

For an antisymmetric $B(x)$ the vector potential in Landau gauge is an even function with $A_y(-x) = A_y(x)$. Consequently the system supports normalizable (near) zero-energy states that are "one sided" in momentum space as shown in Fig. 1. There are two types of momentum-space anisotropy evident in these spectra: (a) The B-induced zero modes occur only for $q = k_y - K(K') < 0$ in both valleys and (b) the $q < 0$ spectrum near K' supports an additional pair of zero modes due to the undercoordinated atoms at the zigzag edges (the total orbital degeneracy of the $q < 0$ spectrum is actually four in this region). The additional low-energy modes bridge the K' and K points where they smoothly evolve into the field-induced zero modes in the opposite valley. In either case the transition from $q < 0$ to $q > 0$ marks a crossover where the zero-energy degrees of freedom hybridize to produce a pair of particle-hole symmetric propagating modes that are confined to the domain wall. For p-type doping (as illustrated) this pair of interfacial modes copropagate along $-\hat{y}$. Physically the pair of domain wall modes combine cyclotron orbital states of opposite circulation to confine their motion near the interface.

The dispersion of the outer-edge modes near the right-hand K' valley is particularly instructive. Note that this band is nearly flat for small $q < 0$ but it becomes strongly dispersive with positive group velocity for sufficiently large negative
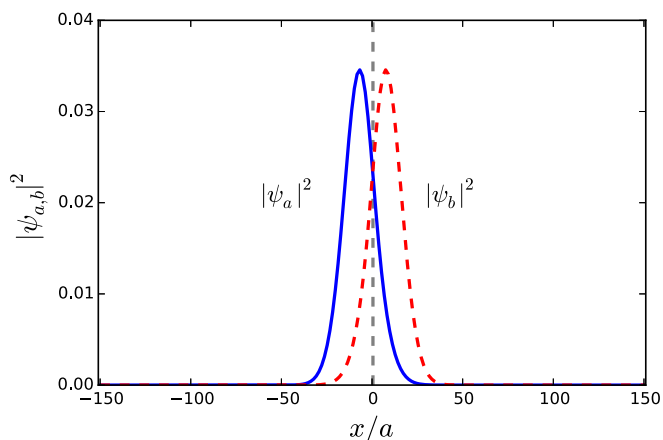
FIG. 2. (Color online) Numerically calculated probability (or charge) density for one of the interface zero-energy modes shown in Fig. 1. The mode is associated with valley K for uniform doping in an antisymmetric magnetic field profile, and ψ_a (solid blue) and ψ_b (red dashed) are the two spinor components. For the other valley, K', the density of the a and b components of the wave function, are interchanged. The x axis is measured in units of the interatomic distance a in graphene.

q. This occurs via hybridization of the sublattice-polarized edge degree of freedom with the Landau zero mode *on the opposite sublattice* when their guiding centers are forced to the outer edges of the ribbon. Note that the antisymmetry of $B(x)$ requires that the guiding centers are forced to opposite outer edges at the same value of the crystal momentum k_y. These dispersive outer edge modes constitute a return path for the topological current induced in the domain wall. These features can be identified in the spatial distribution of the probability (or charge) densities plotted in Figs. 2 and 3.

To summarize, for constant V and antisymmetric B we observe (a) four interface/edge modes at the Fermi energy.
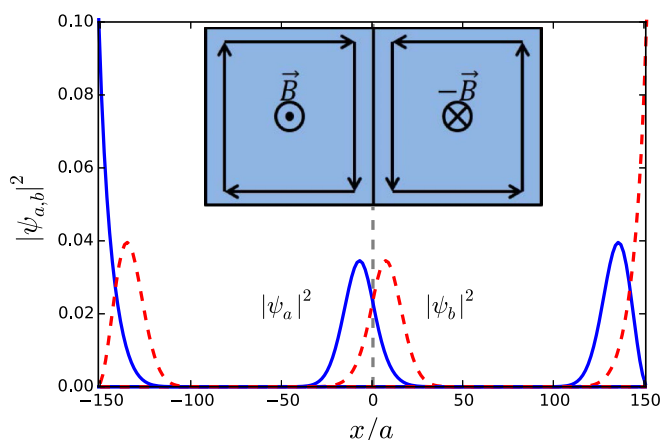

FIG. 3. (Color online) Numerically calculated probability (or charge) density for the zero-energy modes shown in Fig. 1. The two peaks in the center correspond to the interface modes of Fig. 2. The peaks on the left and right side correspond to the edge modes. The solid blue (red dashed) curve represent the ψ_a (ψ_b) spinor component. Inset: Schematic of the current pattern due to opposite cyclotron motions in the two halves of the setup.

(b) A pair of copropagating modes at the domain wall which combine cyclotron motions of opposite circulation. (c) Outer edge modes that hybridize the zeroth Landau level with the zigzag surface state. (d) Valley asymmetry: domain wall modes occur in both valleys but there is support for the outer edge modes only in a single valley. Reversal of the direction of B everywhere will select the other valley.

B. Symmetric B, antisymmetric V

We now consider the opposite limit that occurs with uniform magnetic field and an antisymmetric bias $V(x) = V_o \tanh(x/\ell)$. This creates a graphene pn junction in a uniform field which is the situation studied in two recent experiments [10,11].

The spectrum calculated for this configuration is displayed in Fig. 4 where we plot E-μ as a function of k_y. Here the system is n doped for $x < 0$ and p doped for $x > 0$. Again one finds four dispersing modes at the Fermi energy: two with negative velocity at the domain wall, and two with positive velocity confined on the outer edges. Despite this similarity, the mechanism producing the edge state structure is quite different. We note that the $\sqrt{n}$ signature of the Landau quantization of the Dirac spectrum is observed for $q = k_y - K > 0$ in the K valley but for $q' = k_y - K' < 0$ in the K' valley, i.e., the Landau quantized spectra are both one sided in momentum space, but with opposite senses in the two valleys. In the forbidden regions $q < 0$ and $q' > 0$ the spectrum collapses to a pair of nearly degenerate orbital doublets that connect the two valleys. This degeneracy is exact at $k_y a = \pi/\sqrt{3}$: the energy jump that is produced by the transition $q > 0$ to $q < 0$ (and vice versa for q') is the quantized energy spacing
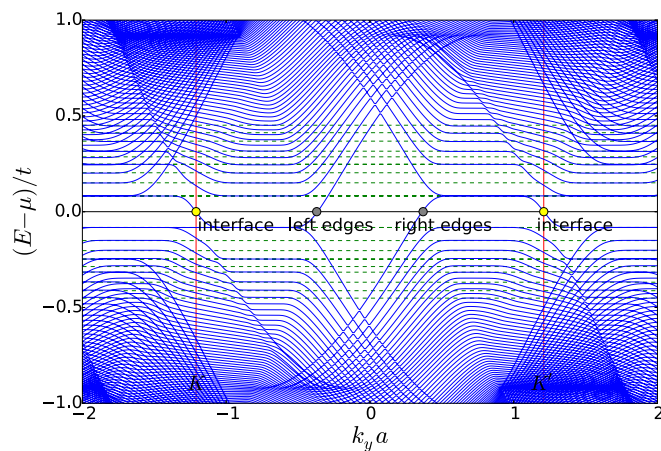

FIG. 4. (Color online) Spectra for the pn junction in a uniform field. The plot gives E-μ as a function of k_y for a geometry where B is constant but $V(x) = V_o \tanh(x/\ell)$. The system supports four edge and interface modes: two positive velocity modes on the outer edges and two negative velocity modes at the domain wall. The flat feature is a zigzag edge state that morphs into the zeroth Landau level. The spectra are one sided, and show graphene character near a shifted neutrality point of one sign of $q = k_y - K$ in one valley and the opposite sign in the other. At $k_y a = \pi/\sqrt{3}$ the spectra are twofold degenerate.
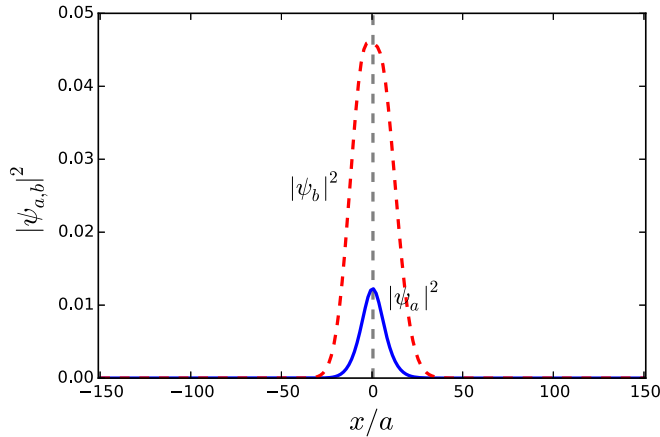
FIG. 5. (Color online) Numerically calculated probability (or charge) density for one of the interface zero-energy modes shown in Fig. 4. The mode is associated with valley K for a graphene pn junction with the potential profile $V(x) = V_o \tanh(x/\ell)$ in a homogeneous perpendicular magnetic field, ψ_a and ψ_b are the two spinor components. For the other valley, K', the density of the a and b components of the wave function, are interchanged.
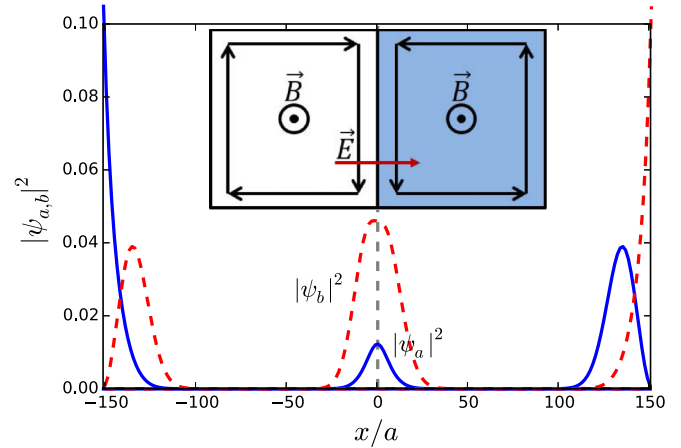

FIG. 6. (Color online) Numerically calculated probability (or charge) density for the zero-energy modes shown in Fig. 4. The two peaks in the center correspond to the interface modes of Fig. 5. The peaks on the left and right side correspond to the edge modes. The solid blue (red dashed) curve represent the ψ_a (ψ_b) spinor component. Inset: Schematic of the current pattern showing the two copropagating modes at the interface between the two halves of the setup. The electric field $\vec{E}$ corresponds to the potential gradient at the pn junction.

between the zeroth and first Landau levels, so all the levels for $k_y a = \pm \pi/\sqrt{3}$ are twofold degenerate.

Here the dispersion of the confined interfacial modes can be understood as a response to the lateral electric field produced in the pn junction. As x crosses zero the scalar potential $V(x)$ switches its sign and the internal electric field $E = -\partial_x V$ is nonzero. Thus a state with drift velocity $\vec{E} \times \vec{B}/B^2$ sees no deflection and can propagate freely. This can be contrasted with the guiding-center mechanism that liberates these modes in the former antisymmetric-B problem where $E = 0$ and one requires the compensation of the circulation in orbits in reversed B fields to produce freely propagating interfacial snake states.

Interestingly, the appearance of dispersive edge modes on the *outer* boundaries follows exactly the same recipe as for the antisymmetric B problem. The guiding center of the Landau zero mode which is sublattice polarized, is forced to the outer edge of the ribbon where it hybridizes with the zigzag surface state on a complementary sublattice to form the one-way dispersive excitation. However, because the B field is constant in this problem, the guiding centers are forced to the outer edges of the ribbon at opposite momenta $\pm k_y$. The entire spectrum of Fig. 4 is then invariant under the combined transformation $E - \mu \rightarrow -(E - \mu)$ and $k_y \rightarrow -k_y$. The probability (or charge) densities associated with the zero modes is plotted in Figs. 5 and 6. We note that the charge density shows a sublattice polarization, favoring the sublattice found in Landau zero mode. This sublattice polarization is captured in the variational approach presented in Sec. VI.

To summarize the main results from this model for the graphene pn junction in a uniform B: (a) Four interface/edge modes at the Fermi energy. (b) Copropagating modes in the domain wall determined by their drift velocity specified by B and the potential gradient in the wall. (c) Conventional outer edge modes that hybridize a Landau zero mode with the surface state.

III. GAUGE EQUIVALENCE VIA NAMBU FORMULATION

It is striking that despite the different microscopic origins of the domain wall solutions and the different structure of the full spectra apparent in Figs. 1 and 4, the basic pattern of the edge state currents is the same. This is evidence of the topological character of these modes. By negating either B or V at the interface we reverse the sign of the Chern number in the first fundamental gap between Landau levels and therefore we require the same pattern of boundary currents. This suggests that the ground states of these two systems can be adiabatically mapped into each other. This conclusion is surprising since the momentum-space structures of their spectra examined in the previous section are evidently controlled by the underlying dynamics which are quite different and in fact incompatible for the two states. In this section we show that their ground states can nonetheless be mapped into each other using a particle-hole extension of the original formulations of both problems. The required mapping is a rotation in the particle and hole degrees of freedom expressed in a Nambu basis. Local gauge transformations in this basis interconvert the two problems at the expense of introducing a fictitious pairing field within the domain wall. In this section we develop a family of such mappings and discuss the consequences of the induced pseudopairing field in Sec. IV.

The problems of Secs. II A and II B are distinguished by the coupling of external potentials to bilinear terms in the fermion operators c and $c^\dagger$. For example, the Peierls phase in Eq. (1) is coupled to nearest-neighbor bilinear terms in the form

$$t e^{i\varphi_{i,j}} c_i^\dagger c_j, \tag{2}$$

while the scalar potential that defines the local doping is coupled through the site density operator

$$V_i (c_i^\dagger c_i - 1/2). \tag{3}$$

Sign reversal of the magnetic field direction negates the exponentiated phase in Eq. (2) while a reversal of the scalar potential flips the sign of the coupling to the net charge operator Eq. (3). Ignoring the physical spin of the electrons, these reversals are introduced by the particle-hole transformation

$$\bar{c} = c^\dagger,$$
$$\bar{c}^\dagger = c, \tag{4}$$

whereby

$$te^{i\varphi_{i,j}} c_i^\dagger c_j \mapsto -te^{i\varphi_{i,j}} \bar{c}_j^\dagger \bar{c}_i = -te^{-i\varphi_{j,i}} \bar{c}_j^\dagger \bar{c}_i,$$
$$V_i(c_i^\dagger c_i - 1/2) \mapsto -V_i(\bar{c}_i^\dagger \bar{c}_i - 1/2). \tag{5}$$

For our application it is useful to collect these operators in two-component spinors that resolve the two degrees of freedom at each Bloch wave vector k,

$$\psi_k = (a_k, b_k) \tag{6}$$

and write the original problem in a doubled Nambu four-component basis $\Psi_k = (\psi_k, \psi_{-k}^\dagger)$,

$$\mathcal{H}_N(k) = (\psi_k^\dagger \quad \psi_{-k}) \begin{pmatrix} \mathcal{H}_k & 0 \\ 0 & -\mathcal{H}_{-k}^* \end{pmatrix} \begin{pmatrix} \psi_k \\ \psi_{-k}^\dagger \end{pmatrix}. \tag{7}$$

When summed over k this theory gives a doubled "redundant" description of the original problem.

Using Eqs. (5) a global rotation in particle-hole space can globally "choose" the signs of B and V. For example, consider a Hamiltonian $\mathcal{H}[V(x), B(x)]$ parametrized by the fields $V(x)$ and $B(x)$. Then define 2×2 Pauli matrices σ_μ acting on the two sublattice degrees of freedom and Σ_μ acting on the particle and hole degrees of freedom in the Nambu representation. A global operator of the form

$$\mathcal{S}(\theta) = \cos\theta\, \mathcal{S}_1 + \sin\theta\, \mathcal{S}_2, \tag{8}$$

where $\mathcal{S}_1 = \sigma_3 \otimes \Sigma_1$ and $\mathcal{S}_2 = \sigma_3 \otimes \Sigma_2$, has the property of formally flipping the signs of V and B everywhere in the manner

$$\mathcal{S}(\theta)^\dagger \mathcal{H}[V(x), B(x)]\mathcal{S}(\theta) = \mathcal{H}[-V(x), -B(x)]. \tag{9}$$

We will discuss the behavior of $\mathcal{S}(\theta = 0) = \mathcal{S}_1$ first and then return to the interpretation of the remaining phase degree of freedom θ.

In an analogous manner, if we promote $\mathcal{S}$ to a local gauge degree of freedom we can introduce a gauge transformation $\mathcal{S}_1(x)$ that *locally* defines the signs of V and B. Specifically, we can use this to interconvert the domain wall configurations of Secs. II A and II B. To keep track of the signs of V and B in the left and right spaces we use a shorthand notation $\mathcal{H}[v_-, v_+; b_-, b_+]$, where $v_\pm$ and $b_\pm$ specify the asymptotic signs of the potential and magnetic field strength. In this notation, $\mathcal{H}[-, +; +, +]$ denotes a situation with $V < 0$ on the left and $V > 0$ on the right, all immersed in a uniform positive field $B > 0$. We now introduce a local gauge transformation

$$\mathcal{S}(x) = \cos\alpha(x)\, \mathbb{I} + i \sin\alpha(x)\, \mathcal{S}_1, \tag{10}$$

where $\alpha(-\infty) \to \pi/2$, $\alpha(\infty) \to 0$, and $\alpha(0) = \pi/4$. This has the effect of implementing a one-sided particle-hole transformation, where the local gauge transformation evolves
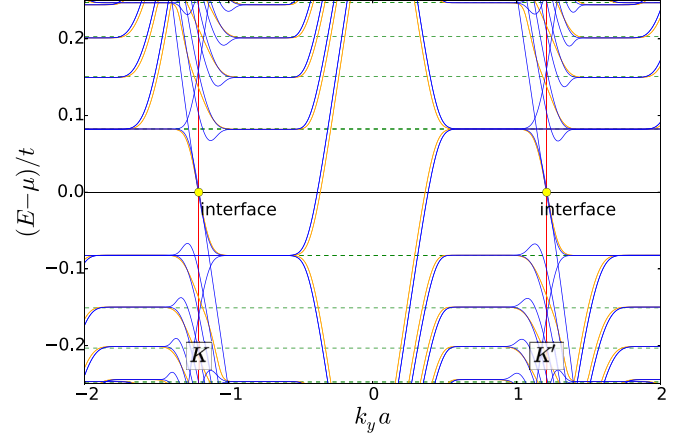

FIG. 7. (Color online) Bogoliubov spectrum for the topological domain wall in graphene corresponding to both Figs. 1 and 4. The spectrum is the particle-hole doubled version of the antisymmetric B spectrum, which is plotted only in the particle channel in Fig. 1. The blue lines correspond to the antisymmetric magnetic field spectrum as shown in Fig. 1; the orange lines correspond to the spectrum of a *pn* junction in a uniform magnetic field as shown in Fig. 4. The horizontal dashed green lines show the Landau-level spectrum for a Dirac particle in a uniform magnetic field for a chemical potential lying symmetrically between the zeroth and the first Landau level.

smoothly through the interface. We retain the original problem for $x \gg 0$ but swap particle and hole amplitudes for $x \ll 0$ to invert the signs of V and B. This transformation is unitary and performs the mapping

$$\mathcal{S}\mathcal{H}[-, +; +, +]\mathcal{S}^\dagger = \mathcal{H}[+, +; -, +], \tag{11}$$

thereby swapping the representation of a *pn* junction in a uniform field with a system with uniform doping in an antisymmetric B field. In the doubled space the ground states can be identified implying that the zero-mode structure is unchanged. In Fig. 7 we overlay the spectra calculated for the two problems in the Nambu representation, illustrating this correspondence.

IV. PAIR FIELD IN THE INTERFACE

An interesting consequence of this mapping is the structure of the spectrum inside the domain wall. The control parameter α varies smoothly through the wall and has the value $\alpha(0) = \pi/4$ exactly at its center. The transformation in Eq. (10) when $\alpha = \pi/4$ is

$$\mathcal{S}_d = (\mathbb{I} + i\sigma_3 \otimes \Sigma_1)/\sqrt{2}$$
$$= \frac{1}{\sqrt{2}} \begin{pmatrix} 1 & 0 & i & 0 \\ 0 & 1 & 0 & -i \\ i & 0 & 1 & 0 \\ 0 & -i & 0 & 1 \end{pmatrix}. \tag{12}$$

As an example, for graphene we explicitly show the complex structure of its sublattice off-diagonal terms:

$$\mathcal{H}_k = \begin{pmatrix} V & \gamma_k^* \\ \gamma_k & V \end{pmatrix}. \tag{13}$$

Inserting this in Eq. (7), in the domain wall the transformed Hamiltonian has the form

$$
\tilde{\mathcal{H}} = \mathcal{S}_d \cdot \mathcal{H}_N(k) \cdot \mathcal{S}_d^\dagger
$$

$$
= \begin{pmatrix} 0 & \mathrm{Re}[\gamma] & -iV & \mathrm{Im}[\gamma] \\ \mathrm{Re}[\gamma] & 0 & \mathrm{Im}[\gamma] & iV \\ iV & \mathrm{Im}[\gamma] & 0 & -\mathrm{Re}[\gamma] \\ \mathrm{Im}[\gamma] & -iV & -\mathrm{Re}[\gamma] & 0 \end{pmatrix}. \quad (14)
$$

Thus, there is a pairing amplitude $\hat{\Delta}[V, \gamma_2]$ defined by the local potential V and the *imaginary part* of the hopping amplitude $\gamma_2 = \mathrm{Im}[\gamma]$. It is a matrix pairing operator acting on the sublattice degrees of freedom. It is symmetric and thereby represents an effective p-wave pairing.

The appearance of an interfacial pair amplitude in the transformed problem can be interpreted as follows. Suppose we introduced the local gauge transformation in the absence of a domain wall. Then in the particle language, electrons would pass through the putative interface undeflected. But in the transformed language this means that an incident electron is converted into a hole with unit probability. This is an Andreev process that requires a pairing field in the Bogoliubov Hamiltonian.

Note that a relation of this form indicates a formal mapping between the problem of Klein tunneling [17] and Andreev reflection at a boundary in the Dirac theory. A closely related observation was made by Beenakker and colleagues a few years ago [18] who noticed that the reflection amplitude for electrons incident on a symmetric graphene pn junction from the n-doped side has a precise analogy with a problem where the particles were actually being Andreev reflected by a contact with a superconductor. This work did not present the problem in a Nambu basis and did not access the physics that we discuss below.

We now look at the symmetries of the original and transformed problem in the domain wall. The original problem can be expressed, using $\gamma_1 = \mathrm{Re}[\gamma]$, $\gamma_2 = \mathrm{Im}[\gamma]$, and suppressing the $\otimes$, as

$$
\mathcal{H}_d = V\sigma_0\Sigma_3 + \gamma_1\sigma_1\Sigma_3 + \gamma_2\sigma_2\Sigma_0, \quad (15)
$$

while after the transformation we have

$$
\tilde{\mathcal{H}}_d = V\sigma_3\Sigma_2 + \gamma_1\sigma_1\Sigma_3 + \gamma_2\sigma_1\Sigma_1. \quad (16)
$$

In both cases the "V" term commutes with the γ_1 and γ_2 terms while the γ_1 and γ_2 terms anticommute. For the pn junction problem, $V = 0$ in the interface. For the antisymmetric B problem V is constant and can be absorbed in the chemical potential. Then because of the anticommutation rules for the γ terms in Eq. (15), zero-energy solutions can only occur when γ_1 and γ_2 simultaneously vanish, as they do precisely at the (projected) Dirac point. In the transformed language this means that a zero-energy solution in the Bogoliubov spectrum for the pseudosuperconductor will similarly require that $\gamma_2 \to 0$ which reveals a momentum-space linear node in the pairing field, consistent with its p-wave symmetry.

The Bogoliubov spectrum is invariant under global $U(1)$ gauge transformations of its matrix-valued pair field $\hat{\Delta}$ in the interface

$$
\hat{\Delta}'(\theta) = e^{-i\theta}\hat{\Delta}(0). \quad (17)
$$

This gauge degree of freedom can be identified with the continuous family of possible transformations in Eq. (8) that interchange the particle and hole degrees of freedom in the Nambu representation. Thus any global $U(1)$ gauge transformation at the interface ($x = 0$) can be absorbed in a redefinition of the global phase angle θ that defines the rotation that is used to switch the particle and hole subspaces. Note that this choice is invisible in the two bounding states but it does appear in the theory of the interface. However, a variation of the phase $\theta(y)$ along the interface is a gauge choice and it is not associated with a physical charge current along its tangent line. To see this we observe that if θ is promoted to a local (i.e., y-dependent) $U(1)$ degree of freedom it also can be eliminated by a local y-dependent gauge transformation back to a number conserving representation at the expense of introducing a connection for operators that transport electrons (holes) along the y direction. Here one can verify that for generic Hamiltonians in the form $\Psi_i^\dagger\Psi_j + \Psi_j^\dagger\Psi_i$ the generalization of Eq. (12)

$$
\mathcal{S}_d(y) = \{\mathbb{I} + i\sigma_3 \otimes [\Sigma_1 \cos\theta(y) + \Sigma_2 \sin\theta(y)]\}/\sqrt{2} \quad (18)
$$

satisfies

$$
(\partial_y S_d^\dagger)S_d + S_d^\dagger\partial_y S_d = 0, \quad (19)
$$

so that any variation $\theta(y)$ in the interfacial pair field disappears completely and leaves no residual signature in the number-conserving blocks of the back-transformed Hamiltonian. The interfacial problem presents the more interesting case of a chiral theory where the Hamiltonian instead has the structure $-i\Psi^\dagger\partial_y\Psi$. Here the connection introduces terms in the Hamiltonian

$$
-iS_d^\dagger\partial_y S_d = [\Sigma_3 + (\Sigma_+ e^{-i\theta} + \Sigma_- e^{i\theta})\sigma_3]\partial_y\theta/2. \quad (20)
$$

The first term commutes with the number conserving blocks and leads to a momentum boost of the spectrum $\propto\partial_y\theta$. The remaining terms anticommute with the number conserving blocks so their effects appear only at higher order $O(\partial_y\theta)^2$ and are unimportant for smoothly varying $\theta(y)$. The momentum boost has no effect on the boundary currents which depend on the number of zero-energy intersections of the chiral branch of the Hamiltonian. The boost can be interpreted as producing a valley polarization within the occupied manifold, however lacking a sharp definition of this polarization (the valleys are connected in the full lattice theory), we expect that any variation $\theta(y)$ has no effects on physically measurable quantities.

V. TOPOLOGICAL CLASSIFICATION

Particle-hole doubling of the domain wall problem promotes its Hamiltonian to a Bogoliubov–de Gennes (BdG) symmetry class. In the original number-conserving representation, this system is gapped breaking time-reversal symmetry ($B \neq 0$), particle-hole symmetry, and chiral symmetry ($\mu \neq 0$). It is described by the Altland-Zirnbauer [19–22] unitary symmetry class A which supports topologically nontrivial ground states in two dimensions which are indexed by an integer-valued invariant $\mathbb{Z}$. The count of the interface states in Secs. II A and II B manifests the mismatch $\Delta\mathbb{Z} = 2$ for the two bounding gapped states across the domain wall.

The Nambu-doubled version of this problem explicitly restores particle-hole symmetry Ξ so that the extended problem can be described by either Altland-Zirnbauer symmetry classes D or C, depending on whether Ξ^2 equals 1 (class D) or -1 (class C). For our application this distinction is important since in the former case the ground state becomes topologically trivial and does not support any symmetry protected modes at its edges or the interfaces. In the latter case (C) the ground state has a $2\mathbb{Z}$ topological classification requiring an *even* number of interfacial/edge modes in the spectrum. In either case an *odd* number of topologically protected edge modes is excluded. Combining the two conditions

$$\Xi^\dagger \Xi = \mathbb{I},$$
$$\{\Xi, \tilde{\mathcal{H}}\} = 0, \tag{21}$$

we have $\Xi = i\sigma_1 \Sigma_2$, so that $\Xi^2 = -1$ and the extended problem is a member of class C.

We have verified this by an explicit calculation of the winding number for the ground state. We carry this out in the number conserving representation where the topological invariants from the particle and hole sectors can be summed. The Chern number ($\mathcal{C}$) for the ground state can be calculated by choosing a chemical potential lying in the first fundamental gap between Landau levels and summing up the Chern numbers for all the individual bands below the chemical potential. The Chern number of the nth Bloch band is

$$\mathcal{C}_n = \frac{1}{2\pi i} \int_{T^2} d^2k [\partial_{k_x} \mathcal{A}_y(\vec{k}) - \partial_{k_y} \mathcal{A}_x(\vec{k})], \tag{22}$$

where the Berry connection

$$\mathcal{A}_\eta(\vec{k}) = \langle n(k_x, k_y)| \partial_{k_\eta} |n(k_x, k_y)\rangle, \tag{23}$$

for $\eta \in \{x, y\}$. Here $|n(k_x, k_y)\rangle$ represents the normalized wave function of the nth Bloch band. We compute the Chern number by discretizing the Brillouin zone (BZ) and summing up the Berry curvature defined on each of the discretized plaquettes [23]. After discretization, the Chern number for the nth band is

$$\tilde{\mathcal{C}}_n = \frac{1}{2\pi i} \sum_{k_x, k_y} F_n(k_x, k_y), \tag{24}$$

where k_x, k_y are within the first BZ,

$$F_n(k_x, k_y) = \ln[U_{k_x}(k_x, k_y) U_{k_y}(k_x + \delta k_x, k_y)$$
$$U_{k_x}(k_x, k_y + \delta k_y)^{-1} U_{k_y}(k_x, k_y)^{-1}], \tag{25}$$

and

$$U_{k_x}(k_x, k_y) = \frac{\det[\Lambda^\dagger(k_x + \delta k_x, k_y) \Lambda(k_x, k_y)]}{|\det[\Lambda^\dagger(k_x + \delta k_x, k_y) \Lambda(k_x, k_y)]|},$$
$$U_{k_y}(k_x, k_y) = \frac{\det[\Lambda^\dagger(k_x, k_y + \delta k_y) \Lambda(k_x, k_y)]}{|\det[\Lambda^\dagger(k_x, k_y + \delta k_y) \Lambda(k_x, k_y)]|}. \tag{26}$$

The column vectors of the matrix $\Lambda(k_x, k_y)$ are given by the Bloch eigenstates $|n(k_x, k_y)\rangle$, where we include all the Bloch bands below the chemical potential. The Bloch eigenstates $|n(k_x, k_y)\rangle$ are obtained by numerically diagonalizing the tight-binding Hamiltonian for the graphene lattice with nearest-neighbor hopping, where the phase of the hopping amplitude is

determined via the Peierls substitution. Assuming that system is of n type and the magnetic field is uniform, adding up the Chern numbers for the particle sector (1) and the hole sector (1), we find that in the ground state $\mathcal{C} = 1 + 1 = 2$. Similarly, we find that $\mathcal{C} = -2$ for a p-type system in a uniform magnetic field. This mismatch of Chern numbers suggests that there should be four topologically protected edge states at the interface defining the *pn* junction. However, since we have artificially doubled the spectrum by going to the Nambu basis, the genuine number of edge states at the interface is two.

The following thought experiment provides an alternative route to demonstrating the equivalence of the $[v_-, v_+, b_-, b_+] = [+, -, +, +]$ and $[+, +, +, -]$ interfaces. The two situations are distinguished by the substitution of $[v_+ > 0, b_+ < 0]$ by $[v_+ < 0, b_+ > 0]$ in the right-hand space. This replacement simultaneously negates the field direction *and* the chemical potential and therefore it leaves the Chern number of the gapped ground state unchanged. This substitution can also be regarded as resulting from the gauge transformation in Eq. (11) imposed on a uniform (V, B) state and implemented on a line *displaced from the physical interface*. Thus this second wall is topologically trivial and does not support any protected interfacial modes. Reducing the separation between the original (physical) $[+, -, +, +]$ interface and the second (fictitious) interface to zero generates the $[+, +, +, -]$ problem without changing the pattern of domain wall currents.

VI. VARIATIONAL SOLUTION FOR THE INTERFACE

Although the full energy spectrum of the graphene honeycomb lattice can be calculated using a tight-binding approximation, additional insight can be obtained from the continuum approximation. In this case a Taylor expansion centered at two nonequivalent Dirac points $\mathbf{K}$ and $\mathbf{K}'$ produces the Dirac-like Hamiltonians $H_K = v_F(\sigma_x \tau_z \hat{p}_x + \sigma_y \hat{p}_y)$, where τ_z acts on the K and K' valley indices and v_F is the Fermi velocity. Together these Hamiltonians can be combined to reproduce a 4×4 two-valley Hamiltonian in terms of the Dirac gamma matrices [24]. Due to the similarities of the two Hamiltonians, here we will only consider the $\mathbf{K}$ point where the Hamiltonian with an external potential $V(x)$ becomes [25–27]

$$\hat{H} = v_F(\vec{\sigma} \cdot \hat{p}) + V(x)\mathbb{I}, \tag{27}$$

where $\vec{\sigma}$ are Pauli matrices in the sublattice basis, $\hat{p} = (\hat{p}_x, \hat{p}_y)$ is the momentum operator, $\mathbb{I}$ is the identity matrix, and $V(x)$ is an external or bias potential associated with an applied electric field. Below we consider the two cases of antisymmetric electric and symmetric magnetic fields and vice versa. In either case the vector potential is written in Landau gauge with $\vec{A} = A_y(x)\hat{y}$ and the Dirac Hamiltonian associated with the K valley and normalized for v_F has the form

$$H = \begin{pmatrix} V(x) & -i\partial_x - (\partial_y - iA_y) \\ -i\partial_x + (\partial_y - iA_y) & V(x) \end{pmatrix}. \tag{28}$$

The solution for the Dirac equation $H\Psi = \epsilon \Psi$ can be written in the Bloch form

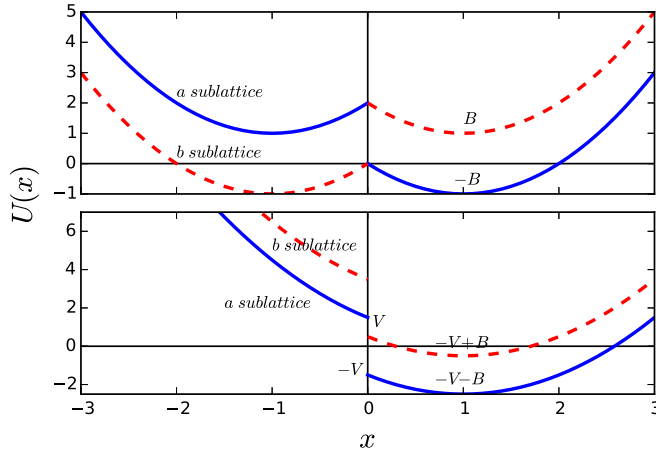$$\psi = e^{ik_y y} \begin{pmatrix} a(x) \\ b(x) \end{pmatrix} \tag{29}$$

FIG. 8. (Color online) Upper panel: potential of the interface created by an antisymmetric magnetic field $B(x) = B \, \text{sign}(x)$. For both sublattices we have a pseudo-Zeeman shifted double parabolic potential. Lower panel: potential of the interface created by an antisymmetric electric bias field $V(x) = -V \text{sign}(x)$. It consists of one parabola, which has a jump at the interface related to the value of the electric field in the pn junction, e.g., as $E = \partial_x V(x)$.

indexed by the conserved wave vector k_y. After this substitution the Dirac equation is rewritten as a pair of coupled second-order equations:

$$\left\{ \left[-\partial_x^2 + (k_y - A_y)^2 \right] \hat{\mathbb{1}} - \partial_x A_y \sigma_z \right\} \psi$$
$$= \left[(\epsilon - V)^2 \hat{\mathbb{1}} + i \partial_x V \sigma_x \right] \psi, \tag{30}$$

which defines a complex matrix-valued potential

$$\mathbb{U} = (k_y - A_y)^2 \hat{\mathbb{1}} - B(x) \sigma_z - i \partial_x V \sigma_x. \tag{31}$$

In the case of an antisymmetric B field with uniform doping, $\partial_x V = 0$ and these equations are decoupled in the sublattice basis so they can be solved separately. For both sublattices we have a particle described by a massive Schrödinger-like equation in a double parabolic potential. In the case when $B(x) = B \, \text{sign}(x)$ the potentials are shown in the upper panel of Fig. 8. The minima in these potentials occur at the values $x = \pm k_y/B$, offset in energy by the pseudo-Zeeman σ_z term in Eq. (31). The a and b sublattice potentials are exchanged by the reflection $x \to -x$.

Equation (28) reveals that these two amplitudes are not independent, but are coupled through the $-i\sigma_x \partial_x$ term in the linearized Hamiltonian. The form of the effective potential $\mathbb{U}$ suggests a useful variational basis for studying the states bound to the domain wall,

$$a(x) = C e^{-(x - x_a)^2/\sigma^2} = C e^{-(x - d)^2/\sigma^2},$$
$$b(x) = C e^{-(x - x_b)^2/\sigma^2} = C e^{-(x + d)^2/\sigma^2}, \tag{32}$$

which are two overlapping Gaussians each of width σ and separated by $2d$; C is a normalization factor. In this variational space the off-diagonal coupling describes a tunneling between states on opposite sides of the interface and with opposite sublattice polarizations. Evaluating the matrix element one

finds

$$\langle a | \mathcal{H} | b \rangle = -\langle b | \mathcal{H} | a \rangle$$
$$= -i \left(\frac{2d}{\sigma^2} - k_y + B \langle |x| \rangle \right) e^{-2d^2/\sigma^2}$$
$$\approx -i \left(\frac{2d}{\sigma^2} \right) e^{-2d^2/\sigma^2}, \tag{33}$$

which is optimized for $d = \sigma/2$ in a gauge where a minimum in the effective potential occurs at $x = 0$ when $k_y = 0$. This demonstrates that the localized variational states are most effectively tunnel coupled at a finite range from the domain wall. The charge density in the lowest energy state is therefore sublattice polarized on opposite sides of the interface as seen in the charge density plotted in Fig. 2. The tunneling Hamiltonian in this variational basis is proportional to σ_y. The energy-optimized state is a coherent combination of these trial basis states forming an eigenfunction of the velocity operator $v_F \sigma_y$ with negative eigenvalue: this is a domain wall state propagating along the $-\hat{y}$ direction. The same physics occurs in the K' valley. In either case the variational solution describes a situation where an incident electron bound in a cyclotron orbit is transmitted through the domain wall where the field is reversed producing a counter circulation of the orbit and liberating the average motion along the tangent line of the wall.

In the case of a homogeneous magnetic field and antisymmetric doping, when $V(x) = -V(-x)$, the a and b sublattice solutions are coupled by the $-i\partial_x V \sigma_x$ term in the potential Eq. (31). For the specific example considered here, when $V(x) = V \text{sign}(x)$ this coupling appears as boundary conditions at the interface,

$$-\partial_x a(0+) + \partial_x a(0-) = i v b(0),$$
$$-\partial_x b(0+) + \partial_x b(0-) = i v a(0), \tag{34}$$

where v is the jump of the electrostatic potential at the interface. The potentials in shown in the lower panel of Fig. 8 again suggest a variational basis. Here the dominant low-energy degree of freedom is a-sublattice polarized in the lowest Landau level on the right side (low potential side) of the interface. It is coupled to an evanescent mode on the right which is b-sublattice polarized penetrating a barrier from the pseudo-Zeeman field, and to evanescent modes on the left penetrating the electrostatic barrier on both sublattices. This physics is captured in the variational basis

$$a(x) = C_a e^{-(x - d)^2/\sigma^2} \quad (x > 0)$$
$$= C_a' e^{x/\ell} \quad (x < 0)$$
$$b(x) = C_b e^{-x/\ell_c} \quad (x > 0)$$
$$= C_b e^{x/\ell} \quad (x < 0), \tag{35}$$

where ℓ_c and ℓ are decay lengths for penetrating the pseudo-Zeeman barrier and the electrostatic barrier, respectively. The matching condition can be written in matrix form

$$\begin{pmatrix} 1/\ell - 2d/\sigma^2 & -iv \\ -iv & 1/\ell + 1/\ell_c \end{pmatrix} \begin{pmatrix} a(0) \\ b(0) \end{pmatrix} = 0. \tag{36}$$

A nontrivial solution occurs when the determinant of the matching matrix is zero, giving

$$d = \frac{\sigma^2}{2\ell}(1 + v'^2 \ell \tilde{\ell}), \tag{37}$$

where $\tilde{\ell} = \ell \ell_c / (\ell + \ell_c)$. The interfacial mode is a vector in the nullspace of Eq. (36),

$$\psi(0) = C \begin{pmatrix} 1 \\ i v \tilde{\ell} \end{pmatrix}. \tag{38}$$

Here $v < 0$ so the group velocity is directed along the $-\hat{y}$ direction. This velocity is evidently proportional to v, consistent with its identification with the classical drift velocity E/B expected in the classical theory of an edge/interface state.

Note also the sublattice asymmetry in this boundary solution: the interfacial mode is not in a velocity eigenstate as was found in the antisymmetric B problem and has its dominant amplitude on the sublattice found in the zero-energy mode (lowest Landau level) in each valley. This is clearly seen in the charge densities calculated for a version of this interface plotted in Fig. 5. The evanescent form of the trial functions in Eq. (35) reflects the different physics operative in the electrostatic barrier. Here an electron bound in a cyclotron orbit is backscattered by an electric field at the interface, weakly penetrating both an electrostatic barrier and a Zeeman barrier due to the sublattice polarization. This behavior is illustrated in Fig. 9.
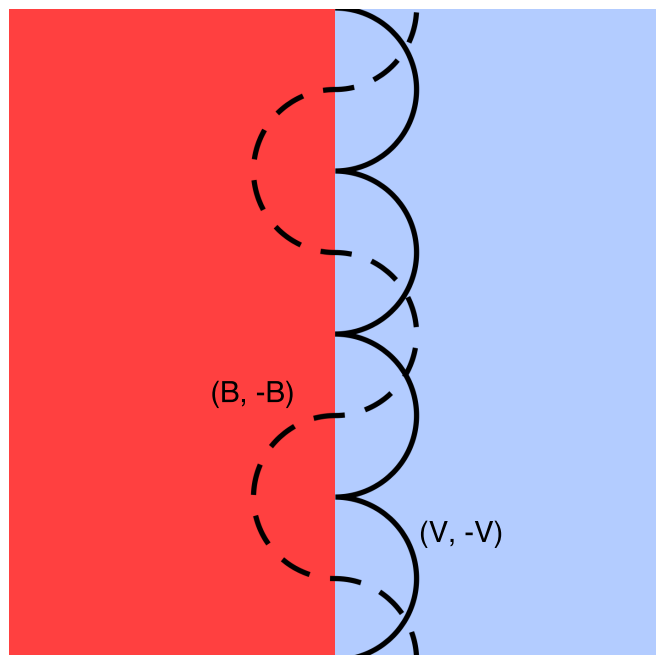

FIG. 9. (Color online) The two different types of domain walls support two different kinds of semiclassical trajectories. Solid line: Skipping orbits typical for the uniform magnetic field case at a $(V, -V)$ domain wall. Dashed lines: Snake orbits typical for a $(B, -B)$ domain wall.

VII. DISCUSSION

Graphene interfaces that support electrostatic barriers (at a pn junction) or field reversal (at a magnetic domain wall) can host confined snake state solutions. The dynamics responsible for these solutions is clearly different in these two situations. For the magnetic domain wall cyclotron orbits of opposite circulation are matched on a boundary to produce an unbound propagating excitation. For the electrostatic barrier a transverse electric field is introduced that reflects an incident mobile carrier to produce a skipping orbit drifting at velocity E/B. Despite these differences the pattern of boundary currents is the same demonstrating the common topological character of both interfaces. We found that these two problems can be mapped onto each other using a particle-hole doubled representation. In this extended basis the two problems are interconverted by a local gauge transformation using the particle and hole degrees of freedom in the Nambu basis. An interesting and unavoidable consequence of this mapping is that a number-conserving version of one problem is the image of a Bogoliubov–de Gennes problem for fermions with an interfacial pair field in the other. This relation offers the interesting possibility of generalizing coherent quantum transport phenomena such as Andreev reflection or Veselago lensing, to a new family of graphene-derived architectures.

Our results imply two "no-go" theorems for this system. First, the gauge-transformed representation of the interfacial problem describes a one-dimensional particle/hole gas coupled by a pairing field with p-wave symmetry. In principle, this class of models can support Majorana excitations in an appropriate parameter regime [28,29]. However, the prospects for realizing such excitations in this setup are remote. We find that the doubled problem has the discrete symmetries of Altland-Zirnbauer symmetry class C so that its gapped ground state is indexed by an *even* integer-valued ($2\mathbb{Z}$) index. Here topological domain wall solutions must appear in pairs, and the possibility of having an unpaired Majorana excitation appearing on the boundary, or at its ends are excluded. This is understandable, since the appearance of such an excitation would not admit an interpretation in the original (number conserving) representation of the same problem. Second, it is intriguing that under the gauge transformation the interfacial problem exhibits an apparent broken $U(1)$ gauge symmetry due to the pseudopairing field. However, this seems not to be associated with any measurable collective effects in the interface: spatial variations of the phase of the order parameter are the images of momentum shifts of the spectrum in the original number-conserving representation of the problem, which is simply a gauge choice. Again, any nontrivial property arising from the pairing field would require a dual interpretation in the number-conserving representation of the same problem. It remains an open question as to whether one might further break the symmetries of the original problem to identify measurable consequences of these symmetries in its gauge transformed image.

Our results highlight several directions for exploiting the structure of the domain wall solutions. It is possible that the sublattice and valley asymmetries found for two problems could be exploited to valley filter ballistic transport in patterned graphene. The two-channel interfacial

solutions may also provide a venue for important one-dimensional interaction effects that are accessible in nonlocal transport measurements between reservoirs bridged by a domain wall. Finally, we also note that while graphene provides a natural starting point for developing this formulation, the conclusions appear to be generally valid for ballistic transport in domain walls separating topologically gapped ground states in a wider class of semiconductor nanostructures.

[1] J. E. Müller, Effect of a Nonuniform Magnetic Field on a Two-Dimensional Electron Gas in the Ballistic Regime, Phys. Rev. Lett. **68**, 385 (1992).

[2] J. Reijniers and F. M. Peeters, Snake orbits and related magnetic edge states, J. Phys.: Condens. Matter **12**, 9771 (2000).

[3] T. K. Ghosh, A. De Martino, W. Häusler, L. Dell'Anna, and R. Egger, Conductance quantization and snake states in graphene magnetic waveguides, Phys. Rev. B **77**, 081404(R) (2008).

[4] S. Park and H. S. Sim, Magnetic edge states in nonuniform magnetic fields, Phys. Rev. B **77**, 075433 (2008).

[5] L. Oroszlany, P. Rakyta, A. Kormanyos, C. J. Lambert, and J. Cserti, Theory of snake states in graphene, Phys. Rev. B **77**, 081403(R) (2008).

[6] L. Brey and H. A. Fertig, Edge States and the quantized Hall effect in graphene, Phys. Rev. B **73**, 195408 (2006).

[7] J. R. Williams, L. DiCarlo, and C. M. Marcus, Quantum Hall effect in a gate controlled *pn* junction in graphene, Science **317**, 638 (2007).

[8] D. A. Abanin, P. A. Lee, and L. S. Levitov, Charge and spin transport at the quantum Hall edge of graphene, Solid State Commun. **143**, 77 (2007).

[9] D. A. Abanin and L. S. Levitov, Quantized transport in graphene *PN* junctions in a magnetic field, Science **317**, 641 (2007).

[10] P. Rickhaus, P. Makk, M.-H. Liu, E. Tóvári, M. Weiss, R. Maurand, K. Richter, and C. Schönenberger, Snake trajectories in ultraclean graphene *pn* junctions, Nat. Commun. **6**, 6470 (2015).

[11] T. Taychatanapat, J. Y. Tan, Y. Yeo, K. Watanabe, T. Taniguchi, and B. Özyilmaz, Conductance oscillations induced by ballistic snake states in a graphene heterojunction, Nat. Commun. **6**, 6093 (2015).

[12] A. H. Castro Neto, F. Guinea, N. M. R. Peres, K. S. Novoselov, and A. K. Geim, Electronic properties of graphene, Rev. Mod. Phys. **81**, 109 (2009).

[13] M. Zarenia, J. M. Pereira, Jr., F. M. Peeters, and G. A. Farias, Snake states in graphene quantum dots in the presence of a *p-n* junction, Phys. Rev. B **87**, 035426 (2013).

[14] P. Carmier, C. Lewenkopf, and D. Ullmo, Graphene *n-p* junction in a strong magnetic field: A semiclassical study, Phys. Rev. B **81**, 241406(R) (2010).

[15] P. Carmier, C. Lewenkopf, and D. Ullmo, Semiclassical magnetotransport in graphene *n-p* junctions, Phys. Rev. B **84**, 195428 (2010).

[16] E. Prada, P. San-Jose, and L. Brey, Zero Landau Level in Folded Graphene Nanoribbons, Phys. Rev. Lett. **105**, 106802 (2010).

[17] M. I. Katsnelson, K. S. Novoselov, and A. K. Geim, Chiral tunneling and the Klein paradox in graphene, Nat. Phys. **2**, 620 (2006).

[18] C. W. J. Beenakker, A. R. Akhmerov, P. Recher, and J. Tworzydlo, Correspondence between Andreev reflection and Klein tunneling in bipolar graphene, Phys. Rev. B **77**, 075409 (2008).

[19] A. Altland and M. R. Zirnbauer, Nonstandard symmetry classes in mesoscopic normal-superconducting hybrid structures, Phys. Rev. B **55**, 1142 (1997).

[20] A. P. Schnyder, S. Ryu, A. Furusaki, and A. W. W. Ludwig, Classification of topological insulators and superconductors in three spatial dimensions, Phys. Rev. B **78**, 195125 (2008).

[21] S. Ryu, A. P. Schnyder, A. Furusaki, and A. W. W. Ludwig, Topological insulators and superconductors: Tenfold way and dimensional hierarchy, New J. Phys. **12**, 065010 (2010).

[22] M. Ezawa, Y. Tanaka, and N. Nagaosa, Topological phase transition without gap closing, Sci. Rep. **3**, 2790 (2013).

[23] T. Fukui, Y. Hatsugai, and H. Suzuki, Chern numbers in discretized Brillouin zone: Efficient method of computing (spin) Hall conductances, J. Phys. Soc. Jpn. **74**, 1674 (2005).

[24] F. V. Kusmartsev and A. M. Tsvelik, Semimetallic properties of a heterojunction, JETP Lett. **42**, 257 (1985).

[25] X. Xu-Guang, Z. Chao, X. Gong-Jie, and C. Jun-Cheng, Electron tunneling in single-layer graphene with an energy gap, Chin. Phys. B **20**, 027201 (2011).

[26] J. V. Gomes and N. M. R. Peres, Tunneling of Dirac electrons through spatial regions of finite mass, J. Phys.: Condens. Matter **20**, 325221 (2008).

[27] M. R. Setare and D. Jahani, Electronic transmission through *p-n* and *n-p-n* junctions of graphene, J. Phys.: Condens. Matter **22**, 245503 (2010).

[28] A. Y. Kitaev, Unpaired Majorana fermions in quantum wires, Phys. Usp. **44**, 131 (2001).

[29] R. P. Tiwari, U. Zülicke, and C. Bruder, Majorana Fermions from Landau Quantization in a Superconductor-Topological-Insulator Hybrid Structure, Phys. Rev. Lett. **110**, 186805 (2013).